

# Electron transport kinetics in the diazotrophic cyanobacterium *Trichodesmium* spp. grown across a range of light levels

Xiaoni Cai · Kunshan Gao · Feixue Fu ·  
Douglas A. Campbell · John Beardall ·  
David A. Hutchins

Received: 14 August 2014 / Accepted: 6 January 2015  
© Springer Science+Business Media Dordrecht 2015

**Abstract** The diazotrophic cyanobacterium *Trichodesmium* is a major contributor to marine nitrogen fixation. We analyzed how light acclimation influences the photophysiological performance of *Trichodesmium* IMS101 during exponential growth in semi-continuous nitrogen fixing cultures under light levels of 70, 150, 250, and 400  $\mu\text{mol photons m}^{-2} \text{s}^{-1}$ , across diel cycles. There were close correlations between growth rate, trichome length, particulate organic carbon and nitrogen assimilation, and cellular absorbance, which all peaked at 150  $\mu\text{mol photons m}^{-2} \text{s}^{-1}$ . Growth rate was light saturated by about 100  $\mu\text{mol photons m}^{-2} \text{s}^{-1}$  and was photoinhibited above 150  $\mu\text{mol photons m}^{-2} \text{s}^{-1}$ . In contrast, the light level ( $I_k$ ) to saturate PSII electron transport ( $e^- \text{ PSII}^{-1} \text{ s}^{-1}$ ) was much higher, in the range of 450–550  $\mu\text{mol photons m}^{-2} \text{s}^{-1}$ , and increased with growth light. Growth rate correlates with the absorption cross section as well as with absorbed photons per cell, but not to electron transport per PSII; this disparity suggests that numbers of PSII in a cell, along with the energy allocation between two photosystems and the state transition mechanism underlie the changes in growth rates. The rate of

state transitions after a transfer to darkness increased with growth light, indicating faster respiratory input into the inter-system electron transport chain.

**Keywords** Light · Electron transport · *Trichodesmium* · State transition

## Abbreviations

PAR	Photosynthetically active radiation (400–700 nm)
PSII	Photosystem II
PSI	Photosystem I
PBS	Phycobilisome
PQ	Plastoquinone
PUB	Phycourobilin
PEB	Phycoerythrobilin
PEC	Phycoerythrocyanin
PC	Phycocyanin
ETR	Electron transport rate
POC	Particulate organic carbon
PON	Particulate organic nitrogen

X. Cai · K. Gao (✉)  
State Key Laboratory of Marine Environmental Science, Xiamen  
University, Xiamen, Fujian, China  
e-mail: ksgao@xmu.edu.cn

F. Fu · D. A. Hutchins  
Department of Biological Sciences, University of Southern  
California, 3616 Trousdale Parkway, Los Angeles, CA, USA

D. A. Campbell  
Department of Biology, Mount Allison University, Sackville,  
NB, Canada

J. Beardall  
School of Biological Sciences, Monash University, Clayton,  
VIC 3800, Australia

## Introduction

*Trichodesmium* spp are the most abundant diazotrophic cyanobacteria (Zehr 2011) in oligotrophic tropical and subtropical surface waters (Capone et al. 1997). They release about 50 % of their recently fixed  $\text{N}_2$  as dissolved organic N (DON) (Glibert and Bronk 1994), thereby contributing substantial fertilization to oligotrophic waters. Nitrogenase can be inactivated by  $\text{O}_2$  (Gallon 1992), nevertheless the non-heterocystous *Trichodesmium* produce  $\text{O}_2$  and fix  $\text{N}_2$  under light in the same trichome (Dugdale et al. 1961; Capone et al. 1997). The cells that perform  $\text{N}_2$  fixation functions, known as diazocytes, show induction of respiratory and nitrogen

fixation enzymes (Sandh et al. 2012) and higher rates of N<sub>2</sub> fixation, peaking at midday concurrently with a drop in O<sub>2</sub> evolution (Berman-Frank et al. 2001).

*Trichodesmium* spp are distributed in the upper layers of the euphotic zone in oligotrophic waters, with the highest *Trichodesmium* densities often found at a depth of 20–40 m (Capone et al. 1997). They are often exposed to high levels of solar radiation while forming blooms in surface waters. Previous studies showed that light compensation points for photosynthesis ranged from 100 to 200 μmol photons m<sup>-2</sup> s<sup>-1</sup> (Carpenter and Roenneberg 1995; LaRoche and Breitbart 2005), corresponding to fairly shallow compensation depths. Photosynthesis became saturated across a wide range of PAR (142–687 μmol photons m<sup>-2</sup> s<sup>-1</sup>) (Kana 1993; Villareal 1995; LaRoche and Breitbart 2005), but *Trichodesmium* colonies did not show photoinhibition of O<sub>2</sub> evolution in the field even under natural sunlight up to 2,500 μmol photons m<sup>-2</sup> s<sup>-1</sup> (Carpenter et al. 1993; Lewis et al. 1988). However, light saturation for the cyanobacteria's growth was much lower, ranging from 100 to 180 μmol photons m<sup>-2</sup> s<sup>-1</sup> (Breitbart et al. 2008; Goebel et al. 2008; Garcia et al. 2011). Consequently, *Trichodesmium* may possess unique strategies to cope with different light regimes.

Photoautotrophs can adapt rapidly to light changes by the regulation of the distribution of absorbed energy between PSII and PSI, termed a state transition. Two primary, but not exclusive, mechanisms by which state transitions are controlled in cyanobacteria are “mobile Phycobilisome” (van Thor et al. 1998; Sarcina et al. 2001) or “energy spillover” from PSII to PSI (Bruce et al. 1989). Studies using fluorescence kinetic microscopy (FKM; Küpper et al. 2004) showed that the basal chlorophyll fluorescence yield (F<sub>0</sub>) increased during N<sub>2</sub> fixation, implying a reversible excitonic coupling of an individual phycobiliprotein, in particular phycocouobilin (PUB) (Küpper et al. 2009). Such a rapid reversible switch could change during light acclimations and correlate with measured state transitions in *Trichodesmium* (Andresen et al. 2010).

In this study, we grew *Trichodesmium erythraeum* IMS101 under sub-saturating, saturating, and super-saturating levels of photosynthetically active radiation (PAR) to examine its energy transfer kinetics and photochemical performance when growing at different rates with proportional changes of particulate organic N and C.

## Materials and methods

### Culturing conditions

*Trichodesmium erythraeum* IMS101 was originally isolated from the North Atlantic Ocean. It was maintained in exponential growth phase under 4 different light levels (70, 150, 250,

400 μmol photons m<sup>-2</sup> s<sup>-1</sup> PAR) in YBCII medium (Chen et al. 1996) at 25 °C with a 12 L/12 D cycle (light from 08:00 to 20:00) for at least 20 days prior to the experiments described below. PAR levels of 70, 150, 250, 400 μmol photons m<sup>-2</sup> s<sup>-1</sup> PAR were achieved using neutral density screening within a plant growth chamber (GXZ, Ningbo, China), and the light intensity was measured with a LI-COR 2π PAR sensor (PMA2100, Solar light, USA). The culture medium was diluted every 4 days so that the cell density was maintained within a range of 1 × 10<sup>4</sup> – 5 × 10<sup>4</sup> cells per ml, in an exponential growth phase. Cell densities were determined by measuring the number and the length of the filaments using an inverted microscope and average cell length was determined with a subsample of the culture. The average number of cells per filament was obtained from the averages of filament length and cell length. Three independent cultures under each light level were run and used to measure the growth rate and all subsequent physiological parameters. The specific growth rate (μ, d<sup>-1</sup>) was estimated as  $\mu = (\ln C_2 - \ln C_1) / (t_2 - t_1)$ , where C<sub>1</sub> and C<sub>2</sub> were the cell numbers per ml at time t<sub>1</sub> and t<sub>2</sub>, respectively.

To measure particulate organic carbon (POC) and nitrogen (PON), 100–200 ml samples were filtered onto pre-combusted GF/F filters (450 °C, 5 h), dried at 60 °C and subjected to CHNS/O elemental analyses (PerkinElmer, USA). Blank values of pre-combusted GF/F filters were subtracted to achieve cellular POC or PON. The production rates of POC and PON were derived as follows:

$$\begin{aligned} \text{Production rate (pmol C or N cell}^{-1}\text{d}^{-1}) \\ = \text{content (pmol C or N cell}^{-1}) \times \mu \text{ (d}^{-1}). \end{aligned}$$

### Chlorophyll fluorometry

PSII fluorescence induction profiles from *Trichodesmium erythraeum* IMS101 were measured using a Fluorescence Induction and Relaxation Fluorometer (FIRE, Satlantic, Halifax, Canada) using blue (450 nm with 30 nm bandwidth) to excite chl *a* and green (530 nm with 30 nm bandwidth) to excite phycobilisomes. We applied a saturating (5 × 10<sup>4</sup> μmol photons m<sup>-2</sup> s<sup>-1</sup>), single turnover flash (120 μs) that saturates PSII photochemistry, and generates a fluorescence induction curve, detected with a long-pass cutoff filter at a wavelength of 680 nm. We used MATLAB software to run the FIREWORX script (Audrey Barnett, <http://sourceforge.net/projects/fireworx/>) with instrument-specific light calibration factors (Satlantic) to extract the fluorescence parameters, F<sub>0</sub> and F<sub>M</sub>, the minimal and maximum chlorophyll fluorescence yield in the dark-adapted (8 min) state [arbitrary units (a.u.)]; F<sub>S</sub> and F<sub>M</sub>' , the steady state and maximum chlorophyll fluorescence yield in the light-adapted state; σ<sub>PSII</sub> and σ<sub>PSII</sub>' the effective absorbance cross section of PSII (A<sup>2</sup> quantum<sup>-1</sup>) in the dark- or light-acclimated states; and τ<sub>Qa-</sub>, re-oxidation time of

$Q_a^-$  ( $\mu\text{s}$ ).  $\sigma_{\text{PSII}}$  and  $\tau_{Q_a^-}$  were estimated from the FIRE fluorescence induction and relaxation data following the model of Kolber et al. (1998). The dark-adapted quantum yield was calculated as  $F_v/F_M = (F_M - F_0)/F_M$ ; while the effective quantum yield  $\Phi_{\text{PSII}} = (F_M' - F_S)/F_M'$  for growth light-adapted cells.

### Light response curves

The PSII-specific electron transport rate ( $e^- \text{ PSII}^{-1} \text{ s}^{-1}$ ) of the cells grown under different light levels was estimated as  $\text{ETR}_{\text{PSII}} = \Phi_{\text{PSII}} \times \sigma_{\text{PSII}}' \times \text{PFD}$  (Huot and Babin 2010), where  $\Phi_{\text{PSII}}$  is the effective quantum yield of PSII at the actinic light level; PFD is the actinic light intensity ( $\mu\text{mol photons m}^{-2} \text{ s}^{-1}$ ), applied in increments up to 2,000  $\mu\text{mol photons m}^{-2} \text{ s}^{-1}$  for a duration of 20 s of each light step;  $\sigma_{\text{PSII}}'$  the effective absorption cross section of the photosystem II (PSII) reaction centers measured under the growth light level, using a green excitation flash.

To analyze the PSII electron transport rate curves, the model of Platt et al. (1980),  $\text{ETR} = \text{ETR}_{\text{max}} \times (1 - \exp(-\alpha \times E/\text{ETR}_{\text{max}})) \times \exp(-\beta \times E/\text{ETR}_{\text{max}})$  was employed to obtain the light saturation parameter ( $I_k$ ) and  $\alpha$ , the initial slope of the light curve before the onset of saturation,  $\beta$ , the photoinhibition parameter.

### Diel patterns in photochemical yield of PSII and light-dark relaxation kinetics

To assess the diel variation in the PSII fluorescence parameters of *Trichodesmium* IMS101 cells grown under different light levels, the photochemical measurements were measured every 2 h during a 14 h period (from 1 h before the onset of light to 1 h after the onset of darkness). The cells were harvested from each of their growth light levels and fluorescence induction curves in their light-acclimated state were measured immediately under their respective growth light levels. Subsequently, the cells were placed in darkness and exposed to a series of single turn-over flashes. The fluorescence induction curves achieved steady state after 5 min of darkness in all cases. The dark-adapted state fluorescence parameters were extracted from a fluorescence induction curve recorded after 8 min of darkness.

Light to dark state transitions were analyzed based upon room temperature Chl fluorescence transients (Mullineaux and Allen 1986). The cyanobacterial cells under growth level illumination, which are in state I, transit to state II upon a shift to darkness. The kinetics of state I to state II transitions were determined by monitoring the progressive decrease in  $F_v/F_M$  during the transition to dark. The state transition kinetics were fit using an exponential decay time

series model as follows:  $y = y_0 + a \times \exp(-k \times t)$ , then the  $T_{1/2} = \ln(2)/k$ , where  $T_{1/2}$  is the time required for yield decay to half of its initial value,  $y_0$  is the yield that reached a steady value.

### Optical absorption cross section

Chlorophyll-specific absorption cross section ( $a^*$ ) was measured using the ‘‘quantitative filter technique’’ (Mitchell 1990). Cellular absorption spectra were determined by collecting cells onto GF/F filters, and scanning each filter from 400 to 750 nm using a 1-nm slit width in a spectrophotometer fitted with an integrating sphere (Lambda950, PerkinElmer, USA). The same filters soaked in the medium without cells were used as blanks; all filters were analyzed immediately. The chl-specific absorption coefficient normalized to chl  $a$ ,  $a^*(\lambda)$  ( $\text{m}^2(\text{mg chl } a)^{-1}$ ), was calculated accordingly to

$$a^*(\lambda) = \frac{2.3[\text{OD}_{\text{filt}}(\lambda) - \text{OD}_{\text{filt}}(750)]}{\beta(V/A)(\text{chl } a)}$$

where 2.3 converts from log base 10 to log base e,  $V$  ( $\text{m}^3$ ) is the volume filtered, and  $A$  ( $\text{m}^2$ ) is the sample area on the filter, correction factor ( $\beta$ ) accounts for the amplified optical path length associated with the glass-fiber filter according to Cleveland and Weidemann (1993), ( $\text{chl } a$ ) is the chl  $a$  concentration. For comparison among the different light acclimations, the optical absorption spectrum ( $a^*$ ) was normalized (Ciotti et al. 2002) using the mean absorption ( $\bar{a}^*$ ) computed between 400 and 700 nm following

$$\bar{a}^* = \frac{1}{300} \sum_{400}^{700} a^*(\lambda) \Delta\lambda.$$

The optical absorption cross section normalized to cell numbers ( $\bar{a}_{\text{cell}}^*$ ,  $\mu\text{m}^2 \text{ cell}^{-1}$ ) was calculated as following:

$$\bar{a}_{\text{cell}}^* (\mu\text{m}^2 \text{ cell}^{-1}) = \bar{a}^* (\text{m}^2(\text{mg chl } a)^{-1}) \times \text{chl } a (\text{mg chl } a \text{ cell}^{-1}) \times 10^{12}.$$

The photons absorbed per day was calculated as

$$\text{Absorbed photons} = \bar{a}_{\text{cell}}^* (\mu\text{m}^2 \text{ cell}^{-1}) \times \mu\text{mol photons PAR m}^{-2} \text{ d}^{-1}.$$

The maximum quantum yield of PSII  $e^-$  generated (PSII  $e^-$  generated per unit quanta absorbed) ( $\varphi_m$ ,  $e^- \text{ quanta}^{-1}$ ) was calculated as

$$\varphi_m = \alpha/\bar{a}^* (\text{Falkowski and Raven 2007}),$$

where  $\alpha$  is the initial slope of PSII ETR curve, giving  $\varphi_m$  as ( $e^- \text{ PSII}^{-1} \text{ s}^{-1}/\mu\text{mol photons PAR m}^{-2} \text{ s}^{-1}$ )/( $\text{m}^2 (\text{mg chl } a)^{-1}$ ). Provided each PSII center has a fixed number of chlorophyll molecules (36 chl per PSII reaction center)

(Richier et al. 2012), we can eliminate  $(\text{mg chl } a)^{-1}$  and  $(\text{PSII } e^-)$ , thus obtaining a unit conversion coefficient  $K = 0.0308$ . The unit of  $\varphi_m$  is then  $(\text{PSII } e^- \text{ generated per unit quanta absorbed})$ .

Chl *a* was extracted in 100 % methanol overnight and quantified from the absorption spectra (400–700 nm) obtained with a spectrophotometer according to Ritchie (2006).

## Statistics

The data were expressed as mean values  $\pm$  SD ( $n = 3$ ) for the three independent replicate cultures. Statistical significance of the data was analyzed with one-way ANOVA and Tukey test at a significance level of  $p < 0.05$ .

## Result

### Growth and C:N ratio

The specific growth rates and the trichome length of *Trichodesmium* IMS101 both reached a maximum under a growth light of  $150 \mu\text{mol photons m}^{-2} \text{s}^{-1}$  and then decreased under higher PAR levels (Fig. 1a). The maximum growth rate was  $0.29$  ( $\text{SD} \pm 0.05$ )  $\text{d}^{-1}$ , which coincided with the longest average filament length of  $882$  ( $\text{SD} \pm 78$ )  $\mu\text{m}$ . There was no significant ( $p = 0.113$ ) change in the growth rate between  $150$  and  $250 \mu\text{mol photons m}^{-2} \text{s}^{-1}$  but the growth rate was significantly lower at the sub-saturating  $70 \mu\text{mol photons m}^{-2} \text{s}^{-1}$  ( $p = 0.005$ ) and at the super-saturating  $400 \mu\text{mol photons m}^{-2} \text{s}^{-1}$  ( $p = 0.014$ ), compared to the values at  $150 \mu\text{mol photons m}^{-2} \text{s}^{-1}$ . The filaments were significantly shorter under  $400 \mu\text{mol photons m}^{-2} \text{s}^{-1}$  ( $p < 0.01$ ), but no significant change in trichome length was found among the other 3 light levels. Overall, growth rates correlate well with filament length (Fig. 1b), suggesting a possibility to estimate population growth rates from single-point measures of filament length, at least when the cultures are not nutrient limited. The rates of particulate organic carbon (POC) and particulate organic nitrogen (PON) production both peaked at  $150 \mu\text{mol photons m}^{-2} \text{s}^{-1}$  with values of  $1.92 \pm 0.25$  and  $0.36 \pm 0.04 \text{ pmol cell}^{-1} \text{ d}^{-1}$ , respectively, and were significantly lower at the sub-saturating  $70 \mu\text{mol photons m}^{-2} \text{s}^{-1}$  ( $p = 0.007$ ,  $p = 0.001$ , respectively) and at the super-saturating  $400 \mu\text{mol photons m}^{-2} \text{s}^{-1}$  ( $p < 0.001$ ) (Fig. 2a). The C:N ratio showed the lowest value in the cells grown at  $150 \mu\text{mol photons m}^{-2} \text{s}^{-1}$ , with significantly higher values at sub-saturating light of  $70 \mu\text{mol photons m}^{-2} \text{s}^{-1}$  ( $p = 0.002$ ) and super-saturating  $400 \mu\text{mol photons m}^{-2} \text{s}^{-1}$  ( $p < 0.001$ ) (Fig. 2b).

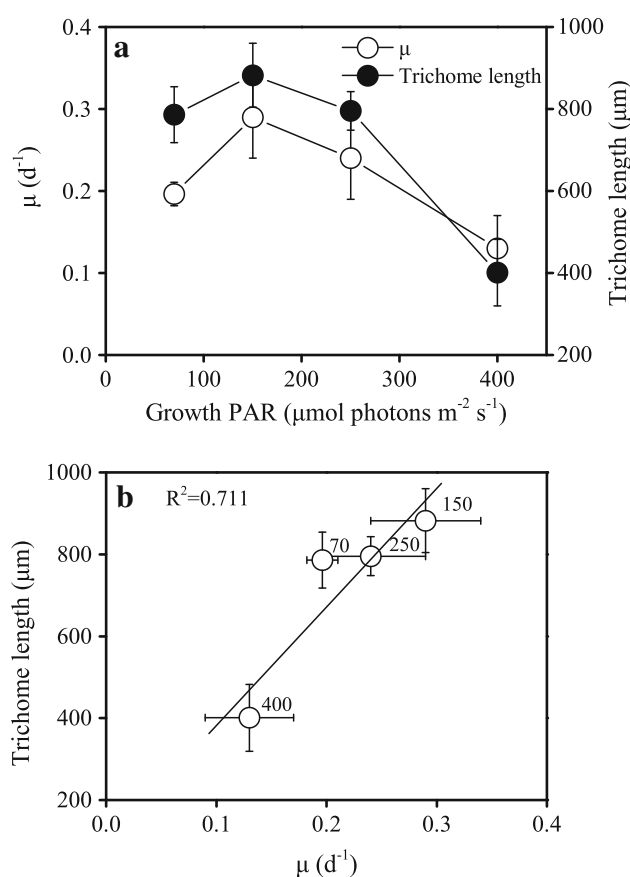


**Fig. 1** **a** Specific growth rate and trichome length of *Trichodesmium erythraeum* IMS101 grown across a range of photosynthetically active radiation (PAR). **b** Trichome length of *T. erythraeum* IMS101 as a function of growth rate. Growth light levels are indicated beside the symbols ( $\mu\text{mol photons m}^{-2} \text{s}^{-1}$ ). The values are mean  $\pm$  SD ( $n = 3$ , triplicate cultures)

### Optical and functional absorbance cross sections

The spectrally averaged chlorophyll-specific optical cross section for light (400–700 nm) normalized to chlorophyll *a*,  $\bar{a}^*$ , was  $0.024$  ( $\text{SD} \pm 0.004$ )  $\text{m}^2 (\text{mg chl } a)^{-1}$  in the cells grown under  $70 \mu\text{mol photons m}^{-2} \text{s}^{-1}$  and  $0.034$  ( $\text{sd} \pm 0.003$ )  $\text{m}^2 (\text{mg chl } a)^{-1}$  in the cells grown under  $400 \mu\text{mol photons m}^{-2} \text{s}^{-1}$  (Fig. 3a), as cellular chlorophyll content dropped with increasing growth light from  $1.3$  ( $\text{SD} \pm 0.2$ )  $\text{pg cell}^{-1}$  for  $70$  to  $0.9$  ( $\text{SD} \pm 0.3$ )  $\text{pg cell}^{-1}$  for  $400 \mu\text{mol photons m}^{-2} \text{s}^{-1}$  cells. Interestingly, growth rate showed a strong correlation with the optical absorption cross section per cell, with the fastest growing cells having the largest optical absorption area per cell (Fig. 3b). The optical absorption spectra revealed the expected series of peaks in the visible wavelengths including chl *a* at  $437$  and  $664$  nm, phycourobilin (PUB) at  $495$  nm, phycoerythrobilin (PEB) at  $545$  nm, phycoerythrocyanin (PEC) at  $569$  nm, and phycocyanin (PC)

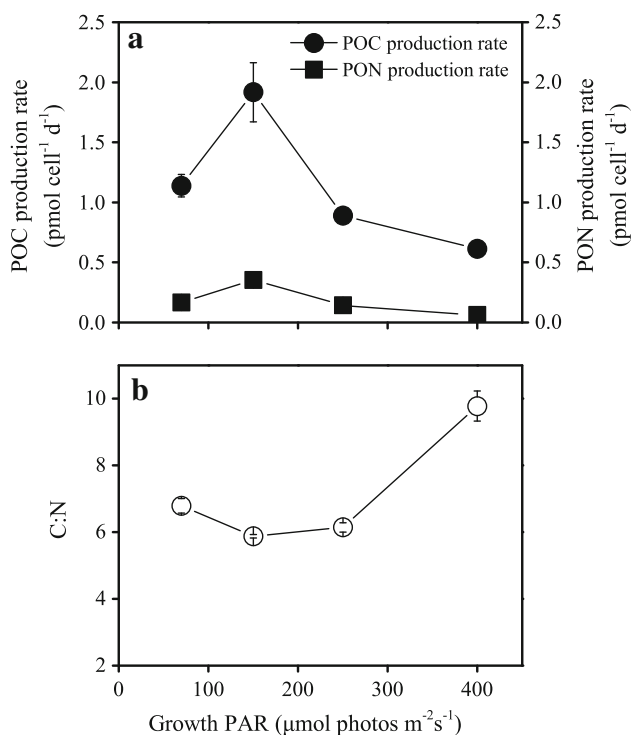


**Fig. 2** **a** Particulate organic carbon (POC) and nitrogen (PON) production rate. **b** The C:N ratio (mol:mol) of *Trichodesmium erythraeum* IMS101 grown under different light levels. The values are mean  $\pm$  SD ( $n = 3$ , triplicate cultures)

at 627 nm (Fig. 3a). The ratio of the maximal peak of PUB to PEB was 1.6:1.0 in the high-light grown cells, and was about 10 % higher than in the low-light grown cells (Fig. 3a).

#### Photochemical performance

The effective photochemical quantum yields for PSII electron transport measured under the growth light levels showed the expected negative correlation with growth light (Fig. 4a), decreasing from about 0.52 (average derived from the blue and green excitations) under the lowest, down to 0.19 under the highest light levels. The apparent yield was moderately higher when measured with the green excitation of phycobilisomes than when measured with the blue direct excitation of chlorophyll, by about 19 % under all growth light levels (Fig. 4a). The functional absorption cross sections of PSII ( $\sigma_{\text{PSII}}'$ ) under all growth light levels were about 3 times larger when measured with the green than with the blue excitation light (Fig. 4b, shown as open symbols). The  $\sigma_{\text{PSII}}'$  measured with green excitation (530 nm with 30 nm bandwidth) decreased by about 36 % during a light to dark transition, averaged across all culture growth light levels (Fig. 4b, shown as circles), reflecting large changes in the excitation connectivity of green-absorbing phycobilisomes to PSII. In contrast, for the blue

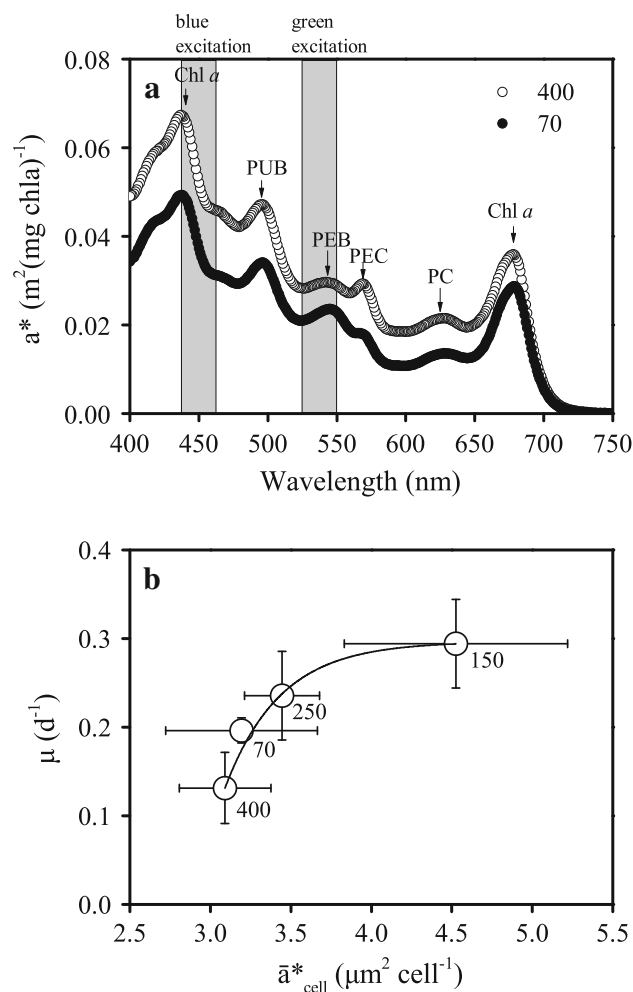


**Fig. 3** **a** Chlorophyll *a* specific absorption spectrum ( $a^*$ ) of *Trichodesmium* grown at 70 and 400  $\mu\text{mol photons m}^{-2}\text{s}^{-1}$ . The absorption peaks of PUB (495 nm), PEB (545 nm), PEC (569 nm), PC (627 nm), and chl *a* (437 and 664 nm) are indicated. Shaded areas indicate the blue (450 nm with 30 nm bandwidth) and green (530 nm with 30 nm bandwidth) excitation regions used for Fluorescence Induction and Relaxation measurements. **b** Growth rate as a function of optical cross section normalized to cell numbers ( $\bar{a}^*_{\text{cell}}$ ), fit with an exponential model (solid line). Growth light levels are indicated beside the symbols ( $\mu\text{mol photons m}^{-2}\text{s}^{-1}$ )

excitation (450 nm with 30 nm bandwidth),  $\sigma_{\text{PSIIblue}}'$  only decreased about 14 % (Fig. 4b, showed as squares), reflecting modest drops in blue excitation delivery to PSII during the state transition, consistent with a modest increase in excitation spillover from PSII to PSI during a light to dark transition. The re-oxidation time of  $\text{Qa}^-$  ( $\tau$ ) measured at 15:00 became longer with increasing growth light levels, reflecting the onset of saturation of electron transport away from PSII under higher growth light levels (Fig. 4c).

Both dark-adapted  $F_V/F_M$  (Fig. 5a, b) and effective quantum yields ( $\Phi_{\text{PSII}}$ , Fig. 5c, d) were higher in the cells grown at lower light levels, with the highest values in the

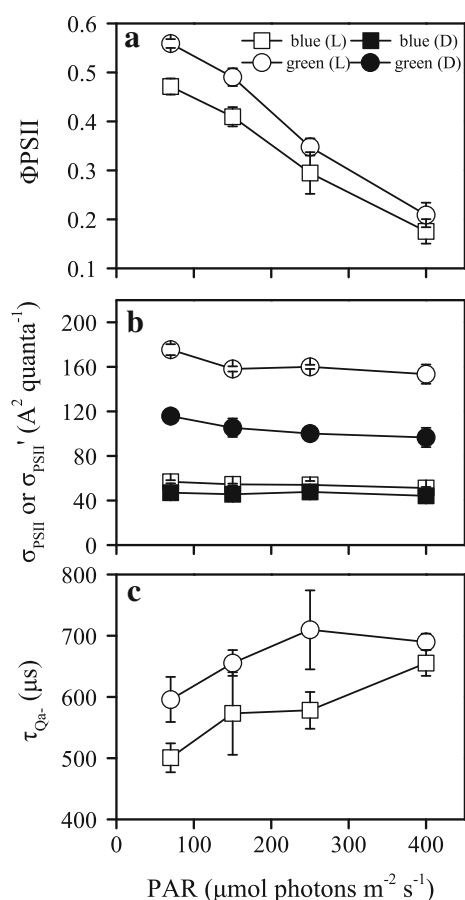


**Fig. 4** **a** The photochemical quantum yield ( $\Phi_{\text{PSII}}$ ), **b** functional absorption cross section of PSII photochemistry measured under dark ( $\sigma_{\text{PSII}}$ ) or under growth light ( $\sigma_{\text{PSII}}'$ ), **c** reoxidation time for  $\text{Qa}^-$  ( $\tau$ ) measured with growth light levels. These parameters were measured in the dark (D) or under growth light levels (L) using either green or blue excitation at 7 h into the light period at 15:00. Some invisible error bars are  $< 7\%$  of the mean values ( $n = 3$ , triplicate cultures)

cells acclimated to the lowest light level. This was true for the yields obtained either with blue (Fig. 5a, c) or green (Fig. 5b, d) excitation lights. The dark-adapted quantum yield  $F_V/F_M$  was lower compared to the effective quantum yields of the cells exposed to the light levels by about 39–52 %, reflecting a transition from dark state II to illuminated state I, consistent with the changes in  $\sigma_{\text{PSII}}'$  to  $\sigma_{\text{PSII}}$  (Fig. 4b). In terms of the diel variations in the yield,  $F_V/F_M$  started to increase 5 h after the onset of illumination in the cells grown under light levels of 70–250  $\mu\text{mol photon m}^{-2} \text{s}^{-1}$  (Fig. 5a, b), and showed a further increase upon the transition back to darkness. The effective yield,  $\Phi_{\text{PSII}}$ , however, increased soon after the onset of illumination in the cells grown under light levels of 150–400  $\mu\text{mol photon m}^{-2} \text{s}^{-1}$  (Fig. 5c, d), with peaks at about 7 h after light onset and thereafter declined with time in the cells grown at light levels above 150  $\mu\text{mol photons m}^{-2} \text{s}^{-1}$  (Fig. 5c, d).

## Kinetics and diel patterns of state transitions

$F_V/F_M$  decreased rapidly when the cells were transferred from their growth light levels to darkness (Fig. 6a). For the cells grown under 400  $\mu\text{mol photons m}^{-2} \text{s}^{-1}$ , the  $F_V/F_M$  declined sharply within 50 s after the onset of darkness and then leveled off. However, for the cells grown under lower light levels, the decline in  $F_V/F_M$  was slower. When the half time ( $T_{1/2}$ ) for the drop of the yield due to the transition from illuminated state I to dark state II was plotted for the cells grown under different light levels over the light period, the higher the growth light level the shorter the  $T_{1/2}$  (Fig. 6b). The  $T_{1/2}$  values increased in late afternoon in the cells grown under the 70 and 150  $\mu\text{mol photons m}^{-2} \text{s}^{-1}$ . This diel pattern disappeared in the cells grown under 400  $\mu\text{mol photons m}^{-2} \text{s}^{-1}$ , which maintained a short state transition  $T_{1/2}$  across the diel cycle.

## Electron transport

The electron transport rate (ETR,  $e^- \text{ PSII}^{-1} \text{ s}^{-1}$ ) plotted versus instantaneous actinic light showed that light use efficiency for the ETR ( $\alpha$ ) and  $\text{ETR}_{\text{max}}$  decreased with increasing growth light levels (Fig. 7a, Table 1). The saturating light levels ( $I_k = \text{ETR}_{\text{max}}/\text{ETR}(\alpha)$ ) were higher in the cells grown under higher light levels (Table 1), while the achieved electron transport rates per PSII under the culture growth light level, which were extracted from the PSII ETR curves, remained steady at  $\sim 80$  ( $e^- \text{ PSII}^{-1} \text{ s}^{-1}$ ) across a wide range of growth light from a growth saturating 150 to a growth inhibitory light level of 400  $\mu\text{mol photons PAR m}^{-2} \text{s}^{-1}$  (Fig. 7b).

The cellular absorbance of photons per day increased with increasing light levels, with the value of  $3 \times 10^{-11}$  mol photons PAR absorbed  $\text{cell}^{-1} \text{d}^{-1}$  at the optimum growth light of 150  $\mu\text{mol photons PAR m}^{-2} \text{s}^{-1}$  (Fig. 8a), but the maximal generation of PSII  $e^-$  per quantum ( $\varphi_m$ ,  $e^- \text{ quanta}^{-1}$ ) decreased from 0.8 to 0.2 with increasing growth light levels (Fig. 8b).

## Discussion

The specific growth rate showed a close correlation with trichome length. The highest growth rate was associated with the highest POC and PON production rates which peaked at 150  $\mu\text{mol photons m}^{-2} \text{s}^{-1}$ . Increased C:N ratios with light levels outside the optimal growth range of 150–250  $\mu\text{mol photons m}^{-2} \text{s}^{-1}$  demonstrated a declining proportion of N assimilation over C assimilation. The C:N ratios obtained under different light levels in this study ranged from 5.88 at the optimal growth light (SD  $\pm 0.05$ ) up to 9.78 (SD  $\pm 0.45$ ) at the highest growth light level,

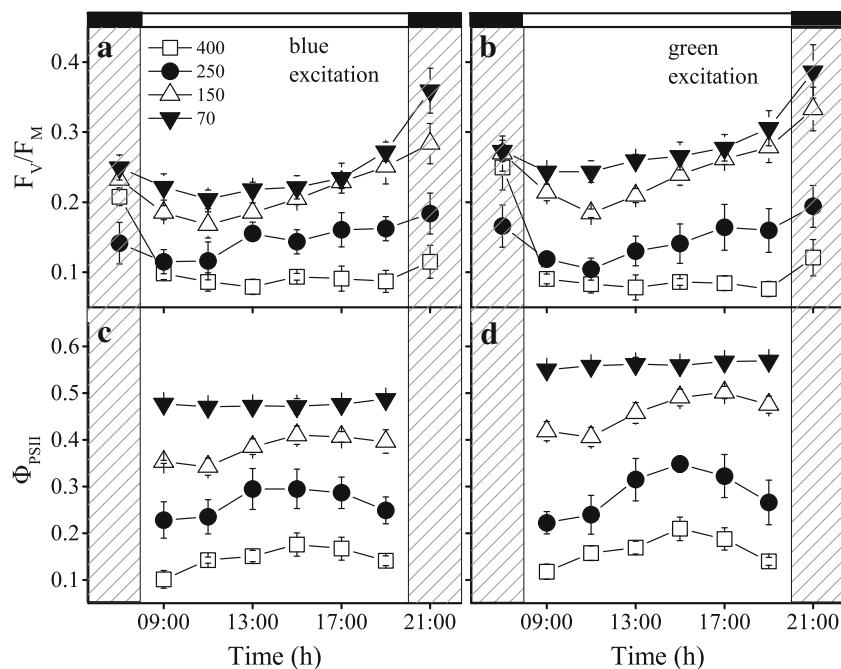


**Fig. 5** Diel changes in dark-adapted quantum yield ( $F_v/F_M$ ) and light-adapted quantum yield ( $\Phi_{\text{PSII}}$ ) of *T. erythraeum* IMS101 grown under the different PAR levels (values and symbols in **a**,  $\mu\text{mol photons m}^{-2} \text{s}^{-1}$ ). The quantum yield ( $\Phi_{\text{PSII}}$ ) was obtained using either blue (450 nm with 30 nm bandwidth) (**a**, **c**) or green (530 nm with 30 nm bandwidth) (**b**, **d**) light for saturating pulse excitation, with

actinic light set at the growth light level for the particular culture. For determination of  $F_v/F_M$  cultures were transferred to darkness for 8 min. The light period started at 08:00 and ended at 20:00 (indicated by the bar on top of the upper graph). The values are mean  $\pm$  SD ( $n = 3$ , triplicate cultures)

somewhat extending the *Trichodesmium* C:N ratios of 4.7–7.3 reported previously (LaRoche and Breitbart 2005). Light regulates the photosynthetic machinery and differentially influences C and N assimilation. It should be noted that the POC and PON production rates do not represent the rates of carbon and nitrogen fixation during the light period, since the POC and PON assimilation are the net carbon and nitrogen retention, after carbon and nitrogen losses either in the dark or during the light period (Mulholland and Bernhardt 2005; Garcia et al. 2011).

Total optical absorption cross section normalized to chlorophyll *a* increased with growth light. These changes reflect a decrease in the “package effect” (Dubinsky et al. 1986), a spectral flattening due to distribution and packing density of pigments within the cell. In the green region of the spectrum, the dip in the cross section values of high-light grown cells could result from both a decreased package effect and to variations in the relative abundance of each of the individual proteins that constitute the ensemble of the phycobilisomes. The *Trichodesmium* cells grown under the high light level showed a higher optical absorption of PUB (phycourobilin), reflected in the elevated peak ratio of PUB to PEB (phycocyanobilin) (Fig. 3a). The changes in apparent composition of the phycobilisome are consistent with those reported

previously (Andresen et al. 2010), implying increased photoprotection associated with the increased PUB (Subramaniam et al. 1999).

PSII function showed strong correlations with growth light levels. The photochemical quantum yield under growth light, as expected, decreased with increased growth light levels and showed diel changes that likely reflect changes in the downstream metabolic removal of electrons from PSII and/or diel changes in the number of functional PSII reaction centers relative to downstream electron sinks (Levitan et al. 2010). The maximal quantum yield for PSII photochemistry also showed diel changes with a dip during late morning (Fig. 5) implying suppressed PSII function during the hours of increased  $\text{N}_2$  fixation (Küpper et al. 2004). The blue light functional absorbance cross section,  $\sigma_{\text{PSIIblue}}$ , for PSII was, as expected, steady across the growth lights since a given PSII has a fixed number of chlorophyll molecules (36 chl per PSII reaction center) (Richier et al. 2012), and the small  $\sigma_{\text{PSIIblue}}$  values (Fig. 4b) primarily represent direct excitation of PSII chlorophylls (Fig. 3a). In contrast,  $\sigma_{\text{PSIIgreen}}$  decreased with increasing growth light, likely reflecting a drop in phycobilisome absorbance per PSII center. Interestingly, growth rate did not correlate with PSII electron transport ( $e^- \text{PSII}^{-1} \text{s}^{-1}$ ) across the different growth light levels (Fig. 7a), but

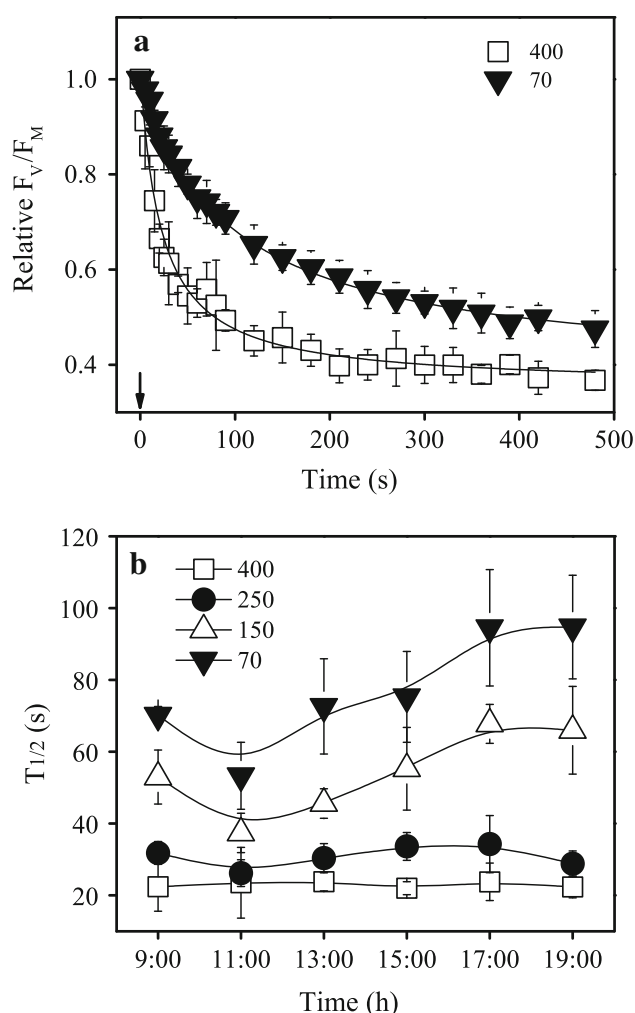


**Fig. 6** **a** Change in  $F_v/F_M$  over time upon a transition to darkness in *T. erythraeum* IMS101. Cells were grown under 70 or 400  $\mu\text{mol photons m}^{-2} \text{s}^{-1}$ . At 11 h into the light period at 19:00, the cells were transferred to darkness (downward arrow). Green saturation pulses were given to probe  $F_M$  every several seconds.  $F_v/F_M$  values were normalized to the values at the beginning of the transition to darkness. **b** Diel variation of the half time for decreases in  $F_v/F_M$  for cultures grown at the different light levels, derived from fitted curves of decreases of relative  $F_v/F_M$  during dark adaptation using an exponential decay time series model. The values are mean  $\pm$  SD ( $n = 3$ , triplicate cultures)

growth rate did correlate closely with the optical absorption cross section per cell (Fig. 3b) and photons absorbed per cell (Fig. 8a). Clearly light capture is the ultimate driver of growth in these photosynthetic and  $\text{N}_2$ -fixing cells. However, the fraction of absorbed photons that trigger PSII electron transport decreased with increasing growth light levels (Fig. 8b), indicating that the cells regulate the light use efficiency to sustain steady electron transport rates per PSII across optimal and super-saturating growth light levels (Fig. 7b). The decoupling of growth rate from achieved electron transport per individual PSII center (Figs. 1, 7)

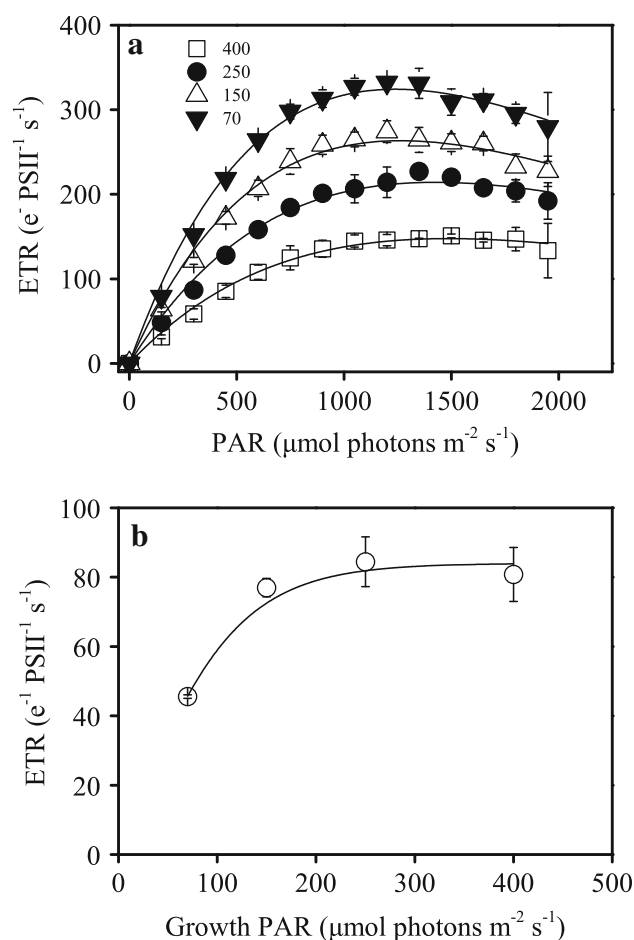


**Fig. 7** **a** Rapid light-response curves of PSII electron transport. Electron transport rate ( $e^- \text{PSII}^{-1} \text{s}^{-1}$ ) versus actinic light for cultures grown at the different light levels (shown in values,  $\mu\text{mol photons m}^{-2} \text{s}^{-1}$ ). Fitted curves are plotted with the solid line using the model from Platt et al. (1980). **b** Achieved PSII electron transport rate at growth light versus culture growth light. PSII ETR values at each growth light level were extracted from three replicate fits of each PSII ETR curve

likely reflects changes in PSII content per cell as well as changes in the cellular quota of organic C and N with increasing growth light levels.

In terms of state transitions, cyanobacteria are usually in state II in the dark, due to respiratory electron flow into the PQ pool, and in state I upon illumination due to high PSI activity withdrawing electrons from the intersystem transport chain, relative to PSII and respiratory activity in the light (Mullineaux and Allen 1986; Mao et al. 2002; Bernát et al. 2012). Cell transfer into darkness, with reduction of the PQ pool by respiratory electron flow, triggers down-regulation of PSII (Campbell et al. 1998), so that the quantum yield of PSII in the dark is lower than that under growth illumination (Figs. 5, 6a). A direct influence of state transitions is also perceptible in the fact that the small  $\sigma_{\text{PSIIblue}}$  changed only modestly during a transition from

**Table 1** The fitted parameters derived from electron transport rate versus irradiance curves [i.e.,  $\alpha$ , the apparent photosynthetic efficiency;  $ETR_{max}$ , the maximum rate of electron transport ( $e^- PSII^{-1}$ s<sup>-1</sup>);  $I_k$ , the initial light saturation point] of cells grown at 70, 150, 250, and 400  $\mu\text{mol photon m}^{-2} \text{s}^{-1}$ , respectively

Growth light ( $\mu\text{mol photons m}^{-2} \text{s}^{-1}$ )	$\alpha$	$ETR_{max}$	$I_k$ ( $\mu\text{mol photons m}^{-2} \text{s}^{-1}$ )
70	$0.71 \pm 0.01^a$	$324 \pm 9^a$	$456 \pm 16^{ab}$
150	$0.57 \pm 0.02^b$	$265 \pm 11^b$	$465 \pm 14^b$
250	$0.41 \pm 0.04^c$	$215 \pm 5^c$	$524 \pm 28^{cd}$
400	$0.27 \pm 0.03^d$	$148 \pm 4^d$	$547 \pm 29^d$

The values are mean  $\pm$  SD ( $n = 3$ , triplicate cultures). The superscripted letters indicate significant difference,  $p < 0.05$

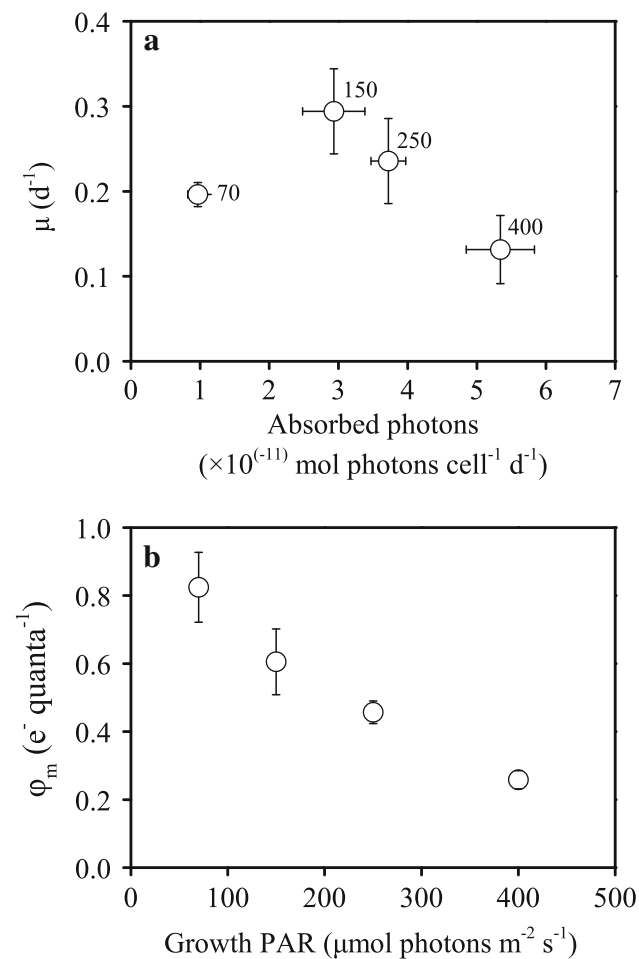


**Fig. 8** **a** Growth rate versus absorbed photons cell<sup>-1</sup> day<sup>-1</sup>, the X-axis plots =  $\bar{\alpha}_{cell}^*$  ( $\mu\text{m}^2 \text{ cell}^{-1}$ )  $\times$   $\mu\text{mol photons PAR m}^{-2} \text{ d}^{-1}$ . Growth light levels are indicated beside the symbols ( $\mu\text{mol photons m}^{-2} \text{ s}^{-1}$ ). **b** A plot showing the correlation between the maximum quantum yield of PSII  $e^-$  generated ( $\phi_m$ ,  $e^- \text{ quanta}^{-1}$ ),  $\phi_m = \alpha/\bar{\alpha}^*$  and culture growth light. The values are mean  $\pm$  SD ( $n = 3$ , triplicate cultures)

light to dark (Fig. 4b) even though the quantum yield of PSII changed sharply over the same transition (Fig. 6a). The  $\sigma_{PSIIgreen}$  decreased slightly with increasing growth light, and dropped sharply during a light to dark transition

(Fig. 4b), showing a drop in the excitation connection between the phycobilisome and the PSII centers, in parallel with the drop in PSII quantum yield (Fig. 6a). The small decline in  $\sigma_{PSIIblue}$  might reflect a drop in the quantum yield for blue light absorbed directly through PSII chlorophyll, but given the spectral bandwidth, it could also reflect changes in phycobilisome excitation transfer, as manifested through the larger drop in green light absorbance cross section (Fig. 4b). These state transition properties imply that *Trichodesmium* might use both a “spillover” of energy from PSII Chl *a* to PSI Chl *a* (McConnell et al. 2002), explaining the modest drop in quantum yield under blue light, and a mobile phycobilisome (Allen and Holmes 1986; Joshua and Mullineaux 2004) with changing coupling with PSII (Küpper et al. 2009; Andresen et al. 2010), explaining the change in  $\sigma_{PSIIgreen}$  during state transitions.

In our experiments, the half time of the state transition,  $T_{1/2}$ , under actinic irradiances was 20–100 s, matching previously published values in other cyanobacterial species (Joshua and Mullineaux 2004; Mullineaux 2014b). The phenomenon that high-light grown cells had faster state transitions was true across the diel cycle (Fig. 6b). However, the  $Qa^-$  re-oxidation rate ( $1/\tau$ ) decreased with increasing growth light levels, implying that the downstream capacity to remove electrons from  $Qa^-$  is lower in the cells grown under the high light levels, since the downstream system was already nearly saturated under the actinic light. Photosynthesis and respiration share the same PQ pool in cyanobacteria and the redox state of the intersystem electron transport chain regulates state transitions (Mullineaux and Allen 1990; Mullineaux 2014a), therefore, a faster state I to dark state II transition, combined with a significant decrease in  $\sigma_{PSIIgreen}$ , could result from faster dark respiration input into the intersystem electron transport chain, possibly combined with a weaker PSII association of phycobiliproteins in the cells grown under high light levels (Mullineaux and Holzwarth 1990; Küpper et al. 2004; Andresen et al. 2010). Regardless of the light levels, the diel changes in the state transition rate showed temporal

patterns similar to  $F_V/F_M$  (Figs. 5a, b, 6b), indicating that the redox poise of the PQ pool correlates with PSII function, since the redox poise of the PQ pool and the overall cellular energy needs are the basic driving forces behind acclimatory changes in the photosynthetic machinery (Sherman et al. 1998; Mullineaux 2014a). Maximal PSII electron transport rate (ETR) per PSII declined with increasing growth light levels (Fig. 7a; Table 1). This reflects the small decrease in  $\sigma_{\text{PSII}}$  with increasing growth light, along with the much larger decrease in  $\Phi_{\text{PSII}}$  with increasing growth light as PSII centers closed as downstream electron transport lagged behind excitation capture under higher growth light intensities. The  $I_k$  values representing the light needed to saturate PSII ETR increased modestly with growth light (Table 1). Interestingly,  $I_k$  for PSII ETR significantly exceeded all growth light levels, showing that PSII electron transport fell well below light saturation across all the growth light levels. In contrast, the  $K_E$  light saturation level for growth rate was only about  $100 \mu\text{mol photons m}^{-2} \text{s}^{-1}$  of PAR, consistent with the PAR range of  $100\text{--}180 \mu\text{mol photons m}^{-2} \text{s}^{-1}$  reported previously in laboratory studies (Breitbarth et al. 2008; Goebel et al. 2008; Garcia et al. 2011), while the growth rate suffered significant photoinhibition by  $400 \mu\text{mol photons m}^{-2} \text{s}^{-1}$ . Taken as a whole, the data suggest a combination of some  $n$ -type (changes in photosynthetic unit numbers) light acclimation with changes in the number of PSI and PSII and phycobilisomes (Falkowski and Owens 1980; Levitan et al. 2010), as reflected in the increase in optical absorbance cross section normalized to chl  $a$ , along with some evidence for a moderate  $\sigma$ -type (changes in photosynthetic unit size) decrease in absorbance cross section attributable to a drop in the size of the green effective cross section measuring delivery of green excitation via phycobilisomes to PSII (Richardson et al. 1983; MacIntyre et al. 2002).

Growth rate could be correlated with differential energy allocations among respiration, carbon or nitrogen assimilation, and photoprotection processes. In our study, the growth rate correlated well with trichome length, the absorption cross section per cell as well as photons absorbed per cell per day, but did not correlate with electron transport rate through each PSII unit. We suggest that the cells at maximum growth rate may have the largest numbers of photosynthetic units, reflected in the largest absorption cross section per cell (Fig. 3b). The decoupling of growth rate from individual PSII activity would thus reflect changes in the stoichiometry of the two photosystems, since *Trichodesmium* has a high activity of cyclic electron transport around PSI, with PSI to PSII ratios ranging from 1.3 to 4 (Berman-Frank et al. 2001; Levitan et al. 2007, 2010). Acclimation by cyanobacteria to different light levels is often manifested in changes in

PSI:PSII ratio (Fujita 1997), and *Trichodesmium* in particular adjusts the stoichiometry of PSII and PSI in favor of increasing PSI when grown under higher light (Levitan et al. 2010). The higher PSI:PSII ratio directs more absorbed light toward cyclic electron flow around PSI that does not directly lead to carbon reduction (Falkowski and Raven 2007).

Our study demonstrated that the diazotrophic cyanobacterium *Trichodesmium* modulates its photosynthetic machinery both during a diel cycle and under increasing light levels, with a faster state transition response under high light. Moreover, it changes the numbers of photosynthetic optical absorption units with changes in growth light.

**Acknowledgments** This study was supported by National Natural Science Foundation (No. 41430967; 41120164007), Joint project of NSFC and Shandong province (Grant No. U1406403), Strategic Priority Research Program of CAS Grant No. XDA11020302, SOA (GASI-03-01-02-04), and China–Japan collaboration project from MOST (S2012GR0290). The visits of D.C., F.F., J.B., and D.H. to Xiamen were supported by MEL’s Visiting Scientist Program and “111” project.

## References

- Allen JF, Holmes NG (1986) A general model for regulation of photosynthetic unit function by protein phosphorylation. *FEBS Lett* 202:175–181
- Andresen E, Lohscheider J, Setlikova E, Adamska I, Simek M, Küpper H (2010) Acclimation of *Trichodesmium erythraeum* ISM101 to high and low irradiance analysed on the physiological, biophysical and biochemical level. *New Phytol* 185:173–188
- Berman-Frank I, Lundgren P, Chen YB, Küpper H, Kolber Z, Bergman B, Falkowski P (2001) Segregation of nitrogen fixation and oxygenic photosynthesis in the marine cyanobacterium *Trichodesmium*. *Science* 294:1534–1537
- Bernát G, Schreiber U, Sendtko E, Stadnichuk IN, Rexroth S, Rögner M, Koenig F (2012) Unique properties vs. common themes: the atypical cyanobacterium *Gloeobacter violaceus* PCC 7421 is capable of state transitions and blue-light-induced fluorescence quenching. *Plant Cell Physiol* 53:528–542
- Breitbarth E, Wohlers J, Kläs J, LaRoche J, Peeken I (2008) Nitrogen fixation and growth rates of *Trichodesmium* IMS-101 as a function of light intensity. *Mar Ecol Prog Ser* 359:25–36
- Bruce D, Brimble S, Bryant DA (1989) State transitions in a phycobilisome-less mutant of the cyanobacterium *Synechococcus* sp. PCC 7002. *Biochim Biophys Acta* 974:66–73
- Campbell D, Hurry V, Clarke AK, Gustafsson P, Oquist G (1998) Chlorophyll fluorescence analysis of cyanobacterial photosynthesis and acclimation. *Microbiol Mol Biol Rev* 62:667–683
- Capone D, Zehr J, Paerl H, Bergman B (1997) *Trichodesmium*, a globally significant marine cyanobacterium. *Science* 276:1221–1227
- Carpenter E, Roenneberg T (1995) The marine planktonic cyanobacteria *Trichodesmium* spp.: photosynthetic rate measurements in the SW Atlantic Ocean. *Mar Ecol Prog Ser* 118:267–273
- Carpenter EJ, Judith M, Capone DG (1993) The tropical diazotrophic phytoplankter *Trichodesmium*: biological characteristics of two common species. *Mar Ecol Prog Ser* 95:295–304

- Chen YB, Zehr JP, Mellon M (1996) Growth and nitrogen fixation of the diazotrophic filamentous nonheterocystous cyanobacterium *Trichodesmium* sp. IMS101 in defined media: evidence for a circadian rhythm. *J Phycol* 32:916–923
- Ciotti AM, Lewis MR, Cullen JJ (2002) Assessment of the relationships between dominant cell size in natural phytoplankton communities and the spectral shape of the absorption coefficient. *Limnol Oceanogr* 47:404–417
- Cleveland JS, Weidemann AD (1993) Quantifying absorption by aquatic particles: a multiple scattering correction for glass-fiber. *Limnol Oceanogr* 38:1321–1327
- Dubinsky Z, Falkowski PG, Wyman K (1986) Light harvesting and utilization by phytoplankton. *Plant Cell Physiol* 27:1335–1349
- Dugdale R, Menzel DW, Ryther JH (1961) Nitrogen fixation in the Sargasso Sea. *Deep-Sea Res* 7:297–300
- Falkowski PG, Owens TG (1980) Light-shade adaptation. Two strategies in marine phytoplankton. *Plant Physiol* 66:592–595
- Falkowski PG, Raven JA (2007) *Aquatic photosynthesis*, 2nd edn. Princeton University Press, New Jersey, pp 237–246
- Fujita Y (1997) A study on the dynamic features of photosystem stoichiometry: accomplishments and problems for future studies. *Photosynth Res* 53:83–93
- Gallon JR (1992) Tansley Review No. 44. Reconciling the incompatible: N<sub>2</sub> fixation and O<sub>2</sub>. *New Phytol* 122:571–609
- Garcia NS, Fu F-X, Breene CL, Bernhardt PW, Mulholland MR, Sohm JA, Hutchins DA (2011) Interactive effects of irradiance and CO<sub>2</sub> on CO<sub>2</sub> fixation and N<sub>2</sub> fixation in the diazotroph *Trichodesmium erythraeum* (cyanobacteria). *J Phycol* 47:1292–1303
- Glibert PM, Bronk DA (1994) Release of dissolved organic nitrogen by marine diazotrophic cyanobacteria, *Trichodesmium* spp. *Appl Environ Microbiol* 60:3996–4000
- Goebel NL, Edwards CA, Carter BJ, Achilles KM, Zehr JP (2008) Growth and carbon content of three different-sized diazotrophic cyanobacteria observed in the subtropical North Pacific. *J Phycol* 44:1212–1220
- Huot Y, Babin M (2010) Overview of fluorescence protocols: theory, basic concepts, and practice. *Chlorophyll a fluorescence in aquatic sciences: methods and applications*, vol 4. Springer, Berlin, pp 31–74
- Joshua S, Mullineaux CW (2004) Phycobilisome diffusion is required for light-state transitions in cyanobacteria. *Plant Physiol* 135:2112–2119
- Kana TM (1993) Rapid oxygen cycling in *Trichodesmium thiebautii*. *Limnol Oceanogr* 38:18–24
- Kolber ZS, Prasil OP, Falkowski PG (1998) Measurements of variable chlorophyll fluorescence using fast repetition rate techniques: defining methodology and experimental protocols. *Biochim Biophys Acta* 1367:88–106
- Küpper H, Ferimazova N, Setlik I, Berman-Frank I (2004) Traffic lights in *Trichodesmium*. Regulation of photosynthesis for nitrogen fixation studied by chlorophyll fluorescence kinetic microscopy. *Plant Physiol* 135:2120–2133
- Küpper H, Andresen E, Wiegert S, Simek M, Leitenmaier B, Setlik I (2009) Reversible coupling of individual phycobiliprotein isoforms during state transitions in the cyanobacterium *Trichodesmium* analysed by single-cell fluorescence kinetic measurements. *Biochim Biophys Acta* 1787:155–167
- LaRoche J, Breitbart E (2005) Importance of the diazotrophs as a source of new nitrogen in the ocean. *J Sea Res* 53:67–91
- Levitan O, Rosenberg G, Setlik I, Setlikova E, Grigel J, Klepetar J, Prasil O, Berman-Frank I (2007) Elevated CO<sub>2</sub> enhances nitrogen fixation and growth in the marine cyanobacterium *Trichodesmium*. *Glob Change Biol* 13:531–538
- Levitan O, Kranz SA, Spungin D, Prasil O, Rost B, Berman-Frank I (2010) Combined effects of CO<sub>2</sub> and light on the N<sub>2</sub>-fixing cyanobacterium *Trichodesmium* IMS101: a mechanistic view. *Plant Physiol* 154:346–356
- Lewis MR, Ulloa O, Platt T (1988) Photosynthetic action, absorption, and quantum yield spectra for a natural population of *Oscillatoria* in the North Atlantic. *Limnol Oceanogr* 33:92–98
- MacIntyre HL, Kana TM, Anning T, Geider RJ (2002) Photoacclimation of photosynthesis irradiance response curve and photosynthetic pigments in microalgae and cyanobacteria. *J Phycol* 38:17–38
- Mao H-B, Li G-F, Ruan X, Wu Q-Y, Gong Y-D, Zhang X-F, Zhao N-M (2002) The redox state of plastoquinone pool regulates state transitions via cytochrome *b<sub>6</sub>f* complex in *Synechocystis* sp. PCC 6803. *FEBS Lett* 519:82–86
- McConnell MD, Koop R, Vasil'ev S, Bruce D (2002) Regulation of the distribution of chlorophyll and phycobilin-absorbed excitation energy in cyanobacteria. A structure-based model for the light state transition. *Plant Physiol* 130:1201–1212
- Mitchell BG (1990) Algorithms for determining the absorption coefficient for aquatic particulates using the quantitative filter technique. In: *Proceedings of SPIE 1302, Ocean Optics X*, p 137
- Mulholland MR, Bernhardt PW (2005) The effect of growth rate, phosphorus concentration, and temperature on N<sub>2</sub> fixation, carbon fixation, and nitrogen release in continuous cultures of *Trichodesmium* IMS101. *Limnol Oceanogr* 50:839–849
- Mullineaux CW (2014a) Co-existence of photosynthetic and respiratory activities in cyanobacterial thylakoid membranes. *Biochim Biophys Acta* 1837:503–511
- Mullineaux CW (2014b) Electron transport and light-harvesting switches in cyanobacteria. *Front Plant Sci* 5:7
- Mullineaux CW, Allen JF (1986) The state 2 transition in the cyanobacterium *Synechococcus* 6301 can be driven by respiratory electron flow into the plastoquinone pool. *FEBS Lett* 205:155–160
- Mullineaux CW, Allen JF (1990) State 1–State 2 transitions in the cyanobacterium *Synechococcus* 6301 are controlled by the redox state of electron carriers between Photosystems I and II. *Photosynth Res* 23:297–311
- Mullineaux CW, Holzwarth AR (1990) A proportion of photosystem II core complexes are decoupled from the phycobilisome in light-state 2 in the cyanobacterium *Synechococcus* 6301. *FEBS Lett* 260:245–248
- Platt T, Gallegos CL, Harrison WG (1980) Photoinhibition of photosynthesis in natural assemblages of marine phytoplankton. *J Mar Res* 38:687–701
- Richardson K, Beardall J, Raven J (1983) Adaptation of unicellular algae to irradiance: an analysis of strategies. *New Phytol* 93:157–191
- Richier S, Macey AI, Pratt NJ, Honey DJ, Moore CM, Bibby TS (2012) Abundances of iron-binding photosynthetic and nitrogen-fixing proteins of *Trichodesmium* both in culture and *in situ* from the North Atlantic. *PLoS One* 7:e35571
- Ritchie RJ (2006) Consistent sets of spectrophotometric chlorophyll equations for acetone, methanol and ethanol solvents. *Photosynth Res* 89:27–41
- Sandh G, Xu L, Bergman B (2012) Diazocyte development in the marine diazotrophic cyanobacterium *Trichodesmium*. *Microbiology* 158:345–352
- Sarcina M, Tobin MJ, Mullineaux CW (2001) Diffusion of phycobilisomes on the thylakoid membranes of the cyanobacterium *Synechococcus* 7942: effects of phycobilisome size, temperature, and membrane lipid composition. *J Biol Chem* 276:46830–46834
- Sherman LA, Meunier P, Colón-López MS (1998) Diurnal rhythms in metabolism: a day in the life of a unicellular, diazotrophic cyanobacterium. *Photosynth Res* 58:25–42

- Subramaniam A, Carpenter EJ, Karentz D, Falkowski PG (1999) Bio-optical properties of the marine diazotrophic cyanobacteria *Trichodesmium* spp. *Limnol Oceanogr* 44:608–617
- van Thor JJ, Mullineaux CW, Matthijs HCP, Hellingwerf KJ (1998) Light harvesting and state transitions in cyanobacteria. *Bot Acta* 111:430–443
- Villareal T (1995) Abundance and photosynthetic characteristics of *Trichodesmium* spp. along the Atlantic Barrier Reef at Carrie Bow Cay, Belize. *Mar Ecol* 16:259–271
- Zehr JP (2011) Nitrogen fixation by marine cyanobacteria. *Trends Microbiol* 19:162–173